Transient analysis of variable-speed wind turbines at wind speed disturbances and a pitch control malfunction

R. Melício[a,c], V.M.F. Mendes[b], J.P.S. Catalão[a,c,*]

[a] *Department of Electromechanical Engineering, University of Beira Interior, R. Fonte do Lameiro, 6201-001 Covilha, Portugal*
[b] *Department of Electrical Engineering and Automation, Instituto Superior de Engenharia de Lisboa, R. Conselheiro Emídio Navarro, 1950-062 Lisbon, Portugal*
[c] *Center for Innovation in Electrical and Energy Engineering, Instituto Superior Técnico, Technical University of Lisbon, Av. Rovisco Pais, 1049-001 Lisbon, Portugal*

Received 17 January 2010; received in revised form 14 April 2010

Abstract

As wind power generation undergoes rapid growth, new technical challenges emerge: dynamic stability and power quality. The influence of wind speed disturbances and a pitch control malfunction on the quality of the energy injected into the electric grid is studied for variable-speed wind turbines with different power-electronic converter topologies. Additionally, a new control strategy is proposed for the variable-speed operation of wind turbines with permanent magnet synchronous generators. The performance of disturbance attenuation and system robustness is ascertained. Simulation results are presented and conclusions are duly drawn.
© 2010 Elsevier Ltd. All rights reserved.

Keywords: Wind energy; Power converters; Transient analysis; Power quality

1. Introduction

The use of renewable energy has been increased in the last decade due to the high cost of fossil fuels and the different agreements among the industrialized countries with the aim of reducing carbon dioxide emissions. Particularly, wind power systems are considered as the most cost effective of all the currently exploited renewable sources [1-3]. Indeed, wind energy is the alternative energy source with the most realistic chance to displace large amounts of fossil fuel combustion [4-6]. Thus, there is a growing global demand for wind energy production [7,8].

In Portugal, the wind power goal foreseen for 2010 was established by the government as 3750 MW and that will constitute some 25% of the total installed capacity by 2010 [9]. This value has recently been raised to 5100 MW, by the most recent governmental goals for the wind sector. Hence, Portugal has one of the most ambitious goals in terms of wind power, and in 2006 was the second country in Europe with the highest wind power growth.

* Corresponding author. Tel.: +351 275 329914; fax: +351 275 329972.
E-mail address: catalao@ubi.pt (J.P.S. Catalão).

Power system stability describes the ability of a power system to maintain synchronism and maintain voltage when subjected to severe transient disturbances [10]. As wind energy is increasingly integrated into power systems, the stability of already existing power systems is becoming a concern of utmost importance [11]. Also, network operators have to ensure that consumer power quality is not compromised. Hence, the total harmonic distortion (THD) should be kept as low as possible, improving the quality of the energy injected into the electric grid [12].

The development of power-electronics and their applicability in wind energy extraction allowed for variable-speed operation of the wind turbine [13]. The variable-speed wind turbines are implemented with either doubly fed induction generator (DFIG) or full-power converter. In a variable-speed wind turbine with full-power converter, the wind turbine is directly connected to the generator, which is usually a permanent magnet synchronous generator (PMSG) [14,15].

Harmonic emissions are recognized as a power quality problem for modern variable-speed wind turbines. Understanding the harmonic behavior of variable-speed wind turbines is essential in order to analyze their effect on the electric grids where they are connected [16].

Variable-speed wind turbines usually employ active pitch control [17], where blade pitch angle increases reduce the captured wind power by reducing the angle of attack. The pitch control may have a considerable effect on the dynamical behavior of wind generators. However, previous papers were mainly focused on the transient analysis of variable-speed wind turbines at external grid faults [18]. Instead, this paper focuses on the transient analysis of variable-speed wind turbines at an internal fault, namely a pitch control malfunction, and wind speed disturbances, studying different topologies for the power-electronic converters in what regards the quality of the energy injected into the electric grid, which is one of our new contributions. Additionally, a new control strategy is proposed for the variable-speed operation of wind turbines with PMSG/full-power converter topology, based on fractional-order controllers, which is compared with a classical integer-order control strategy.

This paper is organized as follows. Section 2 presents the modeling for the wind power system with different topologies for the power converters, namely two-level and multilevel converters. Section 3 provides the new fractional-order control strategy. Section 4 provides the power quality evaluation by THD. Section 5 presents the case study, ascertaining the performance of disturbance attenuation and system robustness. Finally, Section 6 outlines the conclusions.

2. Modeling

2.1 Wind turbine

The mechanical power P_{tt} of the wind turbine is given by:

$$P_{tt} = \frac{1}{2}\rho A u^3 c_p \tag{1}$$

where ρ is the air density, A is the area covered by the rotor blades, u is the wind speed value with disturbance, and c_p is the power coefficient.

The power coefficient c_p is a function of the pitch angle θ of rotor blades, and of the tip speed ratio λ, which is the ratio between blade tip speed and wind speed value upstream of the rotor.

For the simulation of a pitch control malfunction, it is considered that the pitch angle control of the blades imposes momentarily the position of wind gust on the blades, i.e., the blades go to the maximum pitch angle. Thus, the pitch angle variation during the malfunction is severe.

The maximum pitch angle $\theta_{\max} = 55^{\circ}$ is given for the minimum power coefficient, given by:

$$c_{p\min} = 0.0025 \tag{2}$$

for the tip speed ratio given by:

$$\lambda = 3.475 \tag{3}$$

During the conversion of wind energy into mechanical energy, various forces (e.g. centrifugal, gravity and varying aerodynamic forces acting on blades, gyroscopic forces acting on the tower) produce various mechanical effects [19]. Those mechanical effects have been modeled by eigenswings mainly due to the following phenomena: asymmetry in the turbine, vortex tower interaction, and eigenswing in the blades.

The mechanical power over the rotor of the wind turbine has been modeled, using the mechanical eigenswings, as a set of harmonic terms multiplied by the power associated with the energy capture from the wind by the blades. Therefore, the mechanical power over the rotor of the wind turbine P_t may be expressed by [19,20]:

$$P_t = P_{tt}\left[1 + \sum_{k=1}^{3} A_k \left(\sum_{m=1}^{2} a_{km}\, g_{km}(t)\right) h_k(t)\right] \tag{4}$$

$$g_{km} = \sin\left(\int_0^t m\,\omega_k(t')\,dt' + \varphi_{km}\right) \tag{5}$$

where k is the kind of the mechanical eigenswing excited in the rotating wind turbine, m is the order of the harmonic of an eigenswing, A_k is the magnitude of the eigenswing k, g_{km} is the distribution of the m-order harmonic in the eigenswing k, a_{km} is the normalized magnitude of g_{km}, h_k is the modulation of eigenswing k, ω_k is the eigenfrequency of the eigenswing k, and φ_{km} is the phase of the m-order harmonic in the eigenswing k. The frequency range of the wind turbine model with mechanical eigenswings is from 0.1 to 10 Hz. The values used for the calculation of P_t are given in Table 1 [20].

"See Table 1 at the end of the manuscript".

2.2 Wind speed

The wind speed usually varies considerably and has a stochastic character. The wind speed variation can be modeled as a sum of harmonics with frequency range 0.1–10 Hz [19]:

$$u = u_0\left[1 + \sum_k A_k \sin(\omega_k\, t)\right] \tag{6}$$

where u_0 is the average wind speed, u is the wind speed value with disturbance.

Hence, the physical wind turbine model is subjected to the disturbance given by the wind speed variation model [20].

2.3 Mechanical drive train

An accurate way to model a mechanical drive train of a variable-speed wind turbine is to model the rotor as a number of equivalent discrete masses connected together by springs and dampers. When the simulated applications are limited to the impact of wind fluctuations, it is usually sufficient to consider the mechanical drive train as a single-mass shaft model because shaft oscillations of the variable-speed wind turbine are not reflected to the grid due to the fast active power control [21]. In transient analysis, however, when the system response to heavy disturbances is analyzed, the rotor must be approximated by at least a two-mass model [22]. One mass represents the wind turbine moment of inertia, and the other mass represents the generator moment of inertia.

The equations for modeling the mechanical drive train are given by:

$$\frac{d\omega_t}{dt} = \frac{1}{J_t}(T_t - T_{dt} - T_{at} - T_{ts}) \tag{7}$$

$$\frac{d\omega_g}{dt} = \frac{1}{J_g}(T_{ts} - T_{dg} - T_{ag} - T_g) \tag{8}$$

where ω_t is the rotor speed of the wind turbine, J_t is the wind turbine moment of inertia, T_t is the mechanical torque, T_{dt} is the resistant torque in the wind turbine bearing, T_{at} is the resistant torque in the hub and blades due to the viscosity of the airflow, T_{ts} is the torque of torsional stiffness, ω_g is the rotor speed of the generator, J_g is the generator moment of inertia, T_{dg} is the resistant torque in the generator bearing, T_{ag} is the resistant torque due to the viscosity of the airflow in the generator, and T_g is the electric torque. Hence, a two-mass model for the mechanical drive train, given by Eqs. (7) and (8), is considered in this paper.

2.4 Generator

The generator considered in this paper is a PMSG. The equations for modeling a PMSG can be found in the literature [23]. Using the motor machine convention, the following equations are considered:

$$\frac{di_d}{dt} = \frac{1}{L_d}[u_d + p\omega_g L_q i_q - R_d i_d] \tag{9}$$

$$\frac{di_q}{dt} = \frac{1}{L_q}[u_q - p\omega_g(L_d i_d + M i_f) - R_q i_q] \tag{10}$$

where i_f is the equivalent rotor current, M is the mutual inductance, p is the number of pairs of poles; and where in dq axes, i_d and i_q are the stator currents, L_d and L_q are the stator inductances, R_d and R_q are the stator resistances, u_d and u_q are the stator voltages. The electric power P_g is given by:

$$P_g = [u_d \quad u_q \quad u_f][i_d \quad i_q \quad i_f]^T \tag{11}$$

In order to avoid demagnetization of permanent magnet in the PMSG, a null stator current $i_d = 0$ is imposed [24].

2.5 Two-level converter

The two-level converter is an AC/DC/AC converter, with six unidirectional commanded insulated gate bipolar transistors (IGBTs) S_{ik} used as a rectifier, and with the same number of unidirectional commanded IGBTs used as an inverter. The rectifier is connected between the PMSG and a capacitor bank. The inverter is connected between this capacitor bank and a second order filter, which in turn is connected to an electric grid. The groups of two IGBTs linked to the same phase constitute a leg k of the converter.

The configuration of the simulated wind power system with two-level converter is shown in Fig. 1.

"See Fig. 1 at the end of the manuscript".

For the switching function of each IGBT, the switching variable γ_k is used to identify the state of the IGBT i in the leg k of the converter. The index i with $i \in \{1,2\}$ identifies the IGBT. The index k with $k \in \{1,2,3\}$ identifies a leg for the rectifier and $k \in \{4,5,6\}$ identifies the inverter one. The two conditions [25-27] for the switching variable of each leg k are given by:

$$\gamma_k = \begin{cases} 1, & (S_{1k} = 1 \text{ and } S_{2k} = 0) \\ 0, & (S_{1k} = 0 \text{ and } S_{2k} = 1) \end{cases} \qquad k \in \{1, \ldots, 6\} \tag{12}$$

The topological restriction for the leg k is given by:

$$\sum_{i=1}^{2} S_{ik} = 1 \qquad k \in \{1, \ldots, 6\} \tag{13}$$

Each switching variable depends on the conduction and blockade states of the IGBTs.

The voltage v_{dc} is modeled by the state equation:

$$\frac{dv_{dc}}{dt} = \frac{1}{C}\left(\sum_{k=1}^{3} \gamma_k i_k - \sum_{k=4}^{6} \gamma_k i_k\right) \tag{14}$$

2.6 Multilevel converter

The multilevel converter is an AC/DC/AC converter, with twelve unidirectional commanded IGBTs S_{ik} used as a rectifier, and with the same number of unidirectional commanded IGBTs used as an inverter. The rectifier is connected between the PMSG and a capacitor bank. The inverter is connected

between this capacitor bank and a second order filter, which in turn is connected to an electric grid. The groups of four IGBTs linked to the same phase constitute a leg k of the converter.

The configuration of the simulated wind power system with multilevel converter is shown in Fig. 2.

"See Fig. 2 at the end of the manuscript".

For the switching function of each IGBT, the switching variable γ_k is used to identify the state of the IGBT i in the leg k of the converter. The index i with $i \in \{1,2,3,4\}$ identifies the IGBT. The index k with $k \in \{1,2,3\}$ identifies the leg for the rectifier and $k \in \{4,5,6\}$ identifies the inverter one. The three valid conditions [25-27] for the switching variable of each leg k are given by:

$$\gamma_k = \begin{cases} 1, & (S_{1k} \text{ and } S_{2k}) = 1 \quad \text{and} \quad (S_{3k} \text{ or } S_{4k}) = 0 \\ 0, & (S_{2k} \text{ and } S_{3k}) = 1 \quad \text{and} \quad (S_{1k} \text{ or } S_{4k}) = 0 \\ -1, & (S_{3k} \text{ and } S_{4k}) = 1 \quad \text{and} \quad (S_{1k} \text{ or } S_{2k}) = 0 \end{cases} \qquad k \in \{1,\ldots,6\} \tag{15}$$

The topological restriction for the leg k is given by:

$$(S_{1k}.S_{2k}) + (S_{2k}.S_{3k}) + (S_{3k}.S_{4k}) = 1 \qquad k \in \{1,\ldots,6\} \tag{16}$$

With the two upper IGBTs in each leg k (S_{1k} and S_{2k}) of the converter it is associated a switching variable Φ_{1k} and also for the two lower IGBTs (S_{3k} and S_{4k}) it is associated a switching variable Φ_{2k}, respectively given by:

$$\Phi_{1k} = \frac{\gamma_k(1+\gamma_k)}{2} \;;\; \Phi_{2k} = \frac{\gamma_k(1-\gamma_k)}{2} \qquad k \in \{1,\ldots,6\} \tag{17}$$

Each switching variable depends on the conduction and blockade states of the IGBTs.

The voltage v_{dc} is the sum of the voltages v_{C1} and v_{C2} in the capacity banks C_1 and C_2, modeled by the state equation:

$$\frac{dv_{dc}}{dt} = \frac{1}{C_1}\left(\sum_{k=1}^{3}\Phi_{1k}i_k - \sum_{k=4}^{6}\Phi_{1k}i_k\right) + \frac{1}{C_2}\left(\sum_{k=1}^{3}\Phi_{2k}i_k - \sum_{k=4}^{6}\Phi_{2k}i_k\right) \tag{18}$$

2.7 Electric grid

A three-phase active symmetrical circuit in series models the electric grid [25,26]. The phase currents injected in the electric network are modeled by the state equation given by:

$$\frac{di_{fk}}{dt} = \frac{1}{L_n}(u_{fk} - R_n\, i_{fk} - u_k) \qquad k = \{4,5,6\} \tag{19}$$

where R_n and L_n are the resistance and the inductance of the electric network, respectively, u_{fk} is the voltage at the filter and u_k is the voltage at the electric network.

3. Control strategy

3.1 Fractional-order controller

A new control strategy based on fractional-order PI^{μ} controllers is proposed for the variable-speed operation of wind turbines with PMSG/full-power converter topology, and its design is more complex than that of classical PI controllers [28]. Fractional calculus theory is a generalization of ordinary differentiation and integration to arbitrary (non-integer) order [29]. Fractional calculus used in mathematical models of the systems can improve the design, properties and controlling abilities in dynamical systems [30].

The fractional-order differentiator can be denoted by a general operator ${}_aD_t^{\mu}$ [31], given by:

$${}_aD_t^{\mu} = \begin{cases} \dfrac{d^{\mu}}{dt^{\mu}}, & \Re(\mu) > 0 \\ 1, & \Re(\mu) = 0 \\ \displaystyle\int_a^t (d\tau)^{-\mu}, & \Re(\mu) < 0 \end{cases} \tag{20}$$

where μ is the order of derivative or integrals, $\Re(\mu)$ is the real part of the μ.

The mathematical definition of fractional derivatives and integrals has been the subject of several descriptions. The most frequently encountered one is called Riemann–Liouville definition, in which the fractional-order integral is given by [32]:

$${}_aD_t^{-\mu}\, f(t) = \frac{1}{\Gamma(\mu)} \int_a^t (t-\tau)^{\mu-1} f(\tau)\, d\tau \tag{21}$$

while the definition of fractional-order derivatives is:

$$ {}_aD_t^{\mu}\ f(t) = \frac{1}{\Gamma(n-\mu)}\ \frac{d^n}{dt^n}\left[\int_a^t \frac{f(\tau)}{(t-\tau)^{\mu-n+1}}\, d\tau\right] \tag{22} $$

where:

$$ \Gamma(x) \equiv \int_0^{\infty} y^{x-1}\ e^{-y}\ dy \tag{23} $$

is the Euler's Gamma function, a and t are the limits of the operation, and μ is the number identifying the fractional-order. In this paper, μ is assumed as a real number that satisfies the restrictions $0 < \mu < 1$. Also, it is assumed that $a = 0$. The following convention is used: ${}_0D_t^{-\mu} \equiv D_t^{-\mu}$.

The other approach is Grünwald–Letnikov definition of fractional-order integral, given by [33]:

$$ {}_aD_t^{-\mu}\ f(t) = \lim_{h\to 0} h^{\mu} \sum_{r=0}^{\frac{t-a}{h}} \frac{\Gamma(\mu+r)}{r!\,\Gamma(\mu)}\ f(t-rh) \tag{24} $$

while the definition of fractional-order derivatives is:

$$ {}_aD_t^{\mu}\ f(t) = \lim_{h\to 0} h^{-\mu} \sum_{r=0}^{\frac{t-a}{h}} (-1)^r \frac{\Gamma(\mu+1)}{r!\,\Gamma(\mu-r+1)}\ f(t-rh) \tag{25} $$

An important property revealed by the Riemann–Liouville and Grünwald–Letnikov definitions is that while integer-order operators imply finite series, the fractional-order counterparts are defined by infinite series [28-31]. This means that integer operators are local operators in opposition with the fractional operators that have, implicitly, a memory of the past events.

The differential equation of the fractional-order PI^{μ} $0 < \mu < 1$ controller is given by:

$$ u(t) = K_p\ e(t) + K_i\ D_t^{-\mu}\ e(t) \tag{26} $$

where K_p is the proportional constant and K_i is the integration constant. Taking $\mu = 1$, a classical PI controller is obtained. The fractional-order PI^{μ} controller is more flexible than the classical PI controller, because it has one more adjustable parameter, which can reflect the intensity of integration [34].

The transfer function of the fractional-order PI^{μ} controller, using the Laplace transform on Eq. (26), is given by:

$$G(s) = K_p + K_i\, s^{-\mu} \tag{27}$$

As mentioned previously, the use of fractional-order controllers can improve controlling abilities, but its design is more complex than that of classical controllers [28,30]. Different design methods have been reported including pole distribution, frequency domain approach, state-space design, and two-stage or hybrid approach, which uses conventional (integer-order) design methods and then improves performance of the designed control system by adding proper fractional-order controller. An alternative design method is presented in [35] based on particle swarm optimization (PSO) algorithm and employment of a novel cost function, which offers flexible control over time domain and frequency domain specifications. Although applications and design methods regard mainly on linear systems, it is possible to use some of the knowledge already attained to envisage it on nonlinear systems, since the performance of fractional-order controllers in the presence of nonlinearity is of great practical interest [36]. In order to examine the ability of fractional-order controllers for the variable-speed operation of wind turbines, this paper follows the tuning rules in [37]. But, it is recognized that a more systematic procedure for controllers design needs further research in order to well develop tuning implementation techniques [38] for a ubiquitous use of fractional-order controllers.

3.2 Converters control

Power converters are variable structure systems, because of the on/off switching of their IGBTs. As mentioned previously, the controllers used in the converters are fractional-order PI^{μ} controllers. Pulse width modulation (PWM) by space vector modulation (SVM) associated with sliding mode is used for controlling the converters.

The sliding mode control strategy presents attractive features such as robustness to parametric uncertainties of the wind turbine and the generator as well as to electric grid disturbances [39].

Sliding mode controllers are particularly interesting in systems with variable structure, such as switching power converters, guaranteeing the choice of the most appropriate space vectors. Their aim is to let the system slide along a predefined sliding surface by changing the system structure.

The power semiconductors present physical limitations that have to be considered during design phase and during performance simulation. Particularly, they cannot switch at infinite frequency. Also, for a finite value of the switching frequency, an error $e_{\alpha\beta}$ will exist between the reference value and the

control value. In order to guarantee that the system slides along the sliding surface $S(e_{\alpha\beta},t)$, it has been proven that it is necessary to ensure that the state trajectory near the surfaces verifies the stability conditions [40] given by:

$$S(e_{\alpha\beta},t)\ \frac{dS(e_{\alpha\beta},t)}{dt}<0 \tag{28}$$

in practice a small error $\varepsilon>0$ for $S(e_{\alpha\beta},t)$ is allowed, due to power semiconductors switching only at finite frequency.

Consequently, a switching strategy has to be considered, given by:

$$-\varepsilon<S(e_{\alpha\beta},t)<+\varepsilon \tag{29}$$

At the simulation level, a practical implementation of the switching strategy considered in Eq. (29) could be accomplished by using hysteresis comparators.

The outputs of the hysteresis comparators are the integer variables $\sigma_{\alpha\beta}=(\sigma_\alpha,\sigma_\beta)$ [40]. For the two-level converter, σ_α and σ_β assume values in the set Ω given by:

$$\Omega\in\{-1,0,1\} \tag{30}$$

The output voltage vectors in the $\alpha\beta$ plane for the two-level converter are shown in Fig. 3.

"See Fig. 3 at the end of the manuscript".

The appropriate vector selection in order to ensure stability for the two-level converter is shown in Table 2.

"See Table 2 at the end of the manuscript".

For the multilevel converter, σ_α and σ_β assume values in the set Ω given by:

$$\Omega\in\{-2,-1,0,1,2\} \tag{31}$$

The output voltage vectors in the $\alpha\beta$ plane for the multilevel converter are shown in Fig. 4.

"See Fig. 4 at the end of the manuscript".

In this control strategy, only when $v_{C1}\neq v_{C2}$ a new vector is selected. The appropriate vector selection in order to ensure stability for the multilevel converter is shown in Table 3, for $v_{C1}>v_{C2}$, and in Table 4, for $v_{C1}<v_{C2}$.

"See Table 3 and Table 4 at the end of the manuscript".

4. Power quality evaluation

In order to evaluate the harmonic content of the current injected in the electrical grid, the THD is considered. The harmonic content of the current is expressed in percentage of the fundamental component. The THD is given by:

$$\text{THD}\,(\%) = 100\,\frac{\sqrt{\sum_{H=2}^{50} X_H^2}}{X_F} \tag{32}$$

where X_H is the root mean square (RMS) value of the total harmonics of the signal, and X_F is the RMS value of its fundamental component.

5. Simulation results

The wind power system simulated has a rated electric power of 900 kW. The mathematical models for the wind power system with the two-level and multilevel converters were implemented in Matlab/Simulink. Table 5 summarizes the wind power system data. The air density is 1.225 kg/m³.

"See Table 5 at the end of the manuscript".

The time horizon considered in the simulation is 7 s. For the fractional-order PI^{μ} controllers, $\mu = 0.7$, $K_p = 50$ and $K_i = 2.6$ are assumed in this paper. The wind speed model considered in this paper is a ramp increase, taking 1.5 s between 5 and 20 m/s, followed by the wind speed given in Eq. (6) with $u_0 = 20$ m/s.

Hence, the wind speed model considered in this paper is:

$$u(t) = \begin{cases} 10\,t, & 0 \le t \le 1.5 \\ 20\left[1 + \sum_k A_k \sin(\omega_k\, t)\right], & t > 1.5 \end{cases} \qquad 0 \le t \le 7 \tag{33}$$

A pitch control malfunction is simulated between 2 and 2.5 s, imposing a total cut-off on the capture of the energy from the wind by the blades.

The speed of the rotor of the wind turbine besides the disturbance due to the malfunction is also disturbed by the mechanical eigenswings. Fig. 5 shows a zoom between 1 and 5 s of the relative generator rotor speed to the turbine rotor speed.

"See Fig. 5 at the end of the manuscript".

Fig. 6 shows the mechanical power over the rotor of the wind turbine disturbed by the mechanical eigenswings, and the electric power of the generator.

"See Fig. 6 at the end of the manuscript".

The pitch angle variation is shown in Fig. 7. The pitch angle is at 55º during pitch control malfunction, corresponding to the position of wind gust on the blades.

"See Fig. 7 at the end of the manuscript".

The power coefficient variation is shown in Fig. 8. The power coefficient is at zero value during pitch control malfunction.

"See Fig. 8 at the end of the manuscript".

The voltage v_{dc} for the two-level converter, considering a classical PI controller and the proposed fractional $PI^{0.7}$ controller, is shown in Fig. 9. The voltage v_{dc} for the multilevel converter, considering a classical PI controller and the proposed fractional $PI^{0.7}$ controller, is shown in Fig. 10.

"See Fig. 9 at the end of the manuscript".

"See Fig. 10 at the end of the manuscript".

Figs. 9 and10 show that the classical PI controller responds with greater drop on the DC voltage at the converter, during pitch control malfunction, in comparison with the fractional one. The voltage drops are always inferior for the multilevel converter, in comparison with the ones for the two-level converter. A comparison between the maximum values for the DC voltage drops is shown in Table 6.

"See Table 6 at the end of the manuscript".

The voltage v_{dc} drops only about 201 V during the pitch control malfunction with the multilevel converter and the proposed fractional $PI^{0.7}$ controller. On the other hand, the voltage v_{dc} drops almost 551 V during the pitch control malfunction with the two-level converter and a classical PI controller. The use of the proposed fractional $PI^{0.7}$ controller ensures that the DC voltage at the converter has a lesser drop, thus improving the system dynamic performance.

The output current with the fractional-order controller for the two-level converter is shown in Fig. 11, and the one for the multilevel converter is shown in Fig. 12.

"See Fig. 11 at the end of the manuscript".

"See Fig. 12 at the end of the manuscript".

The THD of the current injected in the electric grid with the fractional-order controller and a two-level converter is shown in Fig. 13, while the one with the multilevel converter is shown in Fig. 14.

"See Fig. 13 at the end of the manuscript".

"See Fig. 14 at the end of the manuscript".

Table 7 summarizes a comparison between the control strategies in what regards the THD.

"See Table 7 at the end of the manuscript".

The new control strategy, based on fractional-order controllers, improves the performance of disturbance attenuation and system robustness in comparison with the classical PI control strategy. The quality of the energy injected into the electric grid is improved, keeping the THD at a lower level. Accordingly, a minimum value of 0.13% is attained for the THD, considering the proposed fractional-order controller and multilevel converter. Also, it is shown that the current THD for the wind power system with either a two-level or a multilevel converter is lower than 5% limit imposed by IEEE-519 standard [41]. The IEEE-519 standard is used as a guideline for comparison purposes [42].

6. Conclusions

This paper focuses on the transient analysis of variable-speed wind turbines with PMSG/full-power converter topology, simultaneously considering wind speed disturbances and a pitch control malfunction. Also, a new fractional-order control strategy is proposed in this paper, which improves the performance of disturbance attenuation and system robustness in comparison with a classical integer-order control strategy. It is shown that the quality of the energy injected into the electric grid is improved with the proposed fractional-order controller and multilevel converter, keeping the THD at a lower level. Also, it is shown that the current THD for the wind power system with either a two-level or a multilevel converter is lower than 5% limit imposed by IEEE-519 standard.

References

[1] Gonzalez LG, Figueres E, Garcera G, Carranza O. Maximum-power-point tracking with reduced mechanical stress applied to wind-energy-conversion-systems. Appl Energy 2010, doi:10.1016/j.apenergy.2009.11.030.

[2] Yang H, Wei Z, Chengzhi L. Optimal design and techno-economic analysis of a hybrid solar–wind power generation system. Appl Energy 2009;86(2):163–9.

[3] Morales JM, Mínguez R, Conejo AJ. A methodology to generate statistically dependent wind speed scenarios. Appl Energy 2010;87(3):843–55.

[4] Snyder B, Kaiser MJ. A comparison of offshore wind power development in Europe and the U.S.: Patterns and drivers of development. Appl Energy 2009;86(10):1845–56.

[5] Fyrippis I, Axaopoulos PJ, Panayiotou G. Wind energy potential assessment in Naxos Island, Greece. Appl Energy 2010;87(2):577–86.

[6] Xydis G, Koroneos C, Loizidou M. Exergy analysis in a wind speed prognostic model as a wind farm sitting selection tool: A case study in Southern Greece. Appl Energy 2010;86(11):2411–20.

[7] Kwon S-D. Uncertainty analysis of wind energy potential assessment. Appl Energy 2010;87(3):856–65.

[8] Audierne E, Elizondo J, Bergami L, Ibarra H, Probst O. Analysis of the furling behavior of small wind turbines. Appl Energy 2010, doi:10.1016/j.apenergy.2009.11.019.

[9] Estanqueiro A, Castro R, Flores P, Ricardo J, Pinto M, Rodrigues R, Peças Lopes J. How to prepare a power system for 15% wind energy penetration: the Portuguese case study. Wind Energy 2008;11(1):75–84.

[10] Coughlan Y, Smith P, Mullane A, O'Malley M. Wind turbine modelling for power system stability analysis - A system operator perspective. IEEE Trans Power Syst 2007;22(3):929–36.

[11] Ullah NR, Thiringer T. Variable speed wind turbines for power system stability enhancement. IEEE Trans Energy Convers 2007;22(1):52–60.

[12] Carrasco JM, Franquelo LG, Bialasiewicz JT, Galvan E, Guisado RCP, Prats AM, Leon JI, Moreno-Alfonso N. Power-electronic systems for the grid integration of renewable energy sources: A survey. IEEE Trans Ind Electron 2006;53(4):1002–16.

[13] Baroudi JA, Dinavahi V, Knight AM. A review of power converter topologies for wind generators. Renew Energy 2007;32(14):2369–85.

[14] Brahmi J, Krichen L, Ouali A. A comparative study between three sensorless control strategies for PMSG in wind energy conversion system. Appl Energy 2009;86(9):1565–73.

[15] Arifujjaman Md, Iqbal MT, Quaicoe JE. Reliability analysis of grid connected small wind turbine power electronics. Appl Energy 2009;86(9):1617–23.

[16] Tentzrakis ST, Papathanassiou SA. An investigation of the harmonic emissions of wind turbines. IEEE Trans Energy Convers 2007;22(1):150–8.

[17] Nagai BM, Ameku K, Roy JN. Performance of a 3 kW wind turbine generator with variable pitch control system. Appl Energy 2009;86(9):1774–82.

[18] Jauch C. Transient and dynamic control of a variable speed wind turbine with synchronous generator. Wind Energy 2007;10(3):247–69.

[19] Xing ZX, Zheng QL, Yao XJ, Jing YJ. Integration of large doubly-fed wind power generator system into grid. In: Proc. 8th Int. Conf. Electrical Machines and Systems, Nanjing, China, 2005, pp. 1000–1004.

[20] Akhmatov V, Knudsen H, Nielsen AH. Advanced simulation of windmills in the electric power supply. Int J Electr Power Energy Syst 2000;22(6):421–34.

[21] Slootweg JG, de Haan SWH, Polinder H, Kling WL. Aggregated modelling of wind parks with variable speed wind turbines in power system dynamics simulations. In: Proc. 14th Power Systems Computation Conf., Sevilla, Spain, 2002.

[22] Poller MA. Doubly-fed induction machine models for stability assessment of wind farms. In: Proc. IEEE Bologna Power Tech Conf., Bologna, Italy, 2003.

[23] Ong C-M. Dynamic Simulation of Electric Machinery: Using Matlab/Simulink. Prentice-Hall, New Jersey, 1998, pp. 259–350.

[24] Senjyu T, Tamaki S, Urasaki N, Uezato K. Wind velocity and position sensorless operation for PMSG wind generator. In: Proc. 5th Int. Conf. on Power Electronics and Drive Systems, Singapore, 2003, 787–792.

[25] Melício R, Mendes VMF, Catalão JPS. Two-level and multilevel converters for wind energy systems: a comparative study. In: Proc. 13th Int. Power Electronics and Motion Control Conf., EPE-PEMC 2008, Poznań, Poland, 2008, pp. 1682–1687.

[26] Melício R, Mendes VMF, Catalão JPS. Evaluating power quality in wind power generation systems with two-level and multi-level converters. In: Proc. 6th Mediterranean Conf. and Exhibition on Power Generation, Transmission and Distribution, MedPower 2008, Thessaloniki, Greece, 2008.

[27] Silva JF, Pinto SF. In: M.H. Rashid (Ed.), Control Methods for Switching Power Converters, Power Electronics Handbook, New York, 2007, pp. 935–998.

[28] Arijit B, Swagatam D, Ajith A, Sambarta D. Design of fractional-order PI-lambda-D-mu-controllers with an improved differential evolution. Eng Appl Artif Intell 2009;22:343–50.

[29] Podlubny I. Fractional-order systems and PI-lambda-D-mu-controllers. IEEE Trans Autom Control 1999;44(1):208–14.

[30] Jun-Yi C, Bing-Gang C. Design of fractional order controllers based on particle swarm optimization. In: Proc. of IEEE ICIEA 2006, 2006, pp. 1–6.

[31] Calderón AJ, Vinagre BM, Feliu V. Fractional order control strategies for power electronic buck converters. Signal Process 2006;86(10):2803–19.

[32] Ma C, Hori Y. Fractional order control and its application of (PID)-D-alpha controller for robust two-inertia speed control. In: Proc. 4th Int. Power Electronics and Motion Control Conf., Xian, China, 2004, pp. 1477–1482.

[33] Cafagna D. Fractional calculus: a mathematical tool from the past for present engineers. IEEE Ind Electron Mag 2007;1(2):35–40.

[34] Zong K, Li S, Lin X. The application of fractional-order PI control algorithm to the PMSM speed-adjusting system. In: Proc. 3rd Int. Conf. on Intelligent Computing, Qingdao, China, 2007, 660–669.

[35] Zamani M, Karimi-Ghartemani M, Sadati N, Parniani M. Design of fractional order PID controller for an AVR using particle swarm optimization. Control Eng Practice 2009;17(12):1380–7.

[36] Barbosa RS, Machado JAT, Galhano AM. Performance of fractional PID algorithms controlling nonlinear systems with saturation and backlash phenomena. J Vibration and Control 2007;13(9-10):1407–18.

[37] Maione G, Lino P. New tuning rules for fractional PI-alfa controllers. Nonlinear Dynamics 2007;49(1-2):251–7.

[38] Chen YQ, Petras I, Xue D. Fractional order control–a tutorial. In: Proc. 2009 American Control Conference, St. Louis, Missouri, USA, 2009, 1397–1411.

[39] Beltran B, Ahmed-Ali T, Benbouzid MEH. Sliding mode power control of variable-speed wind energy conversion system. IEEE Trans Energy Convers 2008;23(2):551–8.

[40] Pinto S, Silva J. Sliding mode direct control of matrix converters. IET Electr Power Appl 2007;1(3):439–48.

[41] IEEE Guide for Harmonic Control and Reactive Compensation of Static Power Converters, IEEE Standard 519-1992.

[42] Nick TMH, Tan K, Islam S. Mitigation of harmonics in wind turbine driven variable speed permanent magnet synchronous generators. In: Proc. 7th Int. Power Engineering Conf., Singapore, 2005, pp. 1159–1164.

Figure captions

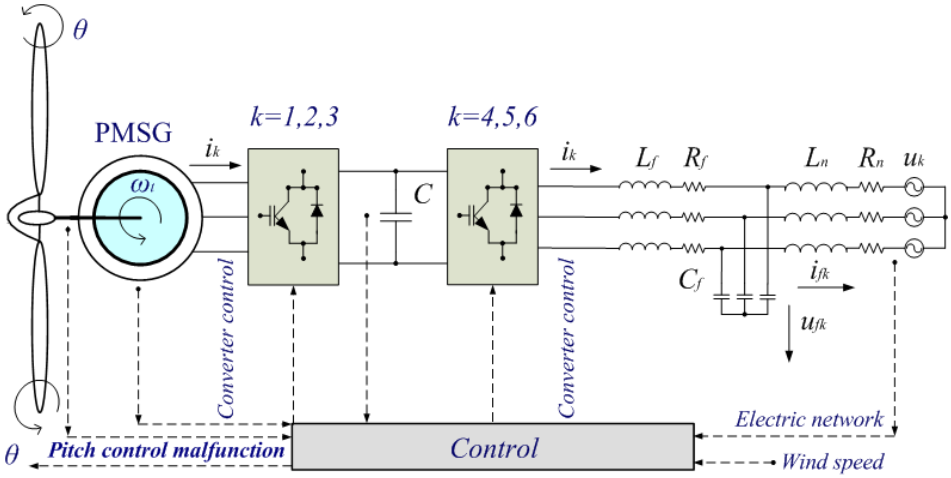

Fig. 1. Wind power system with two-level converter.

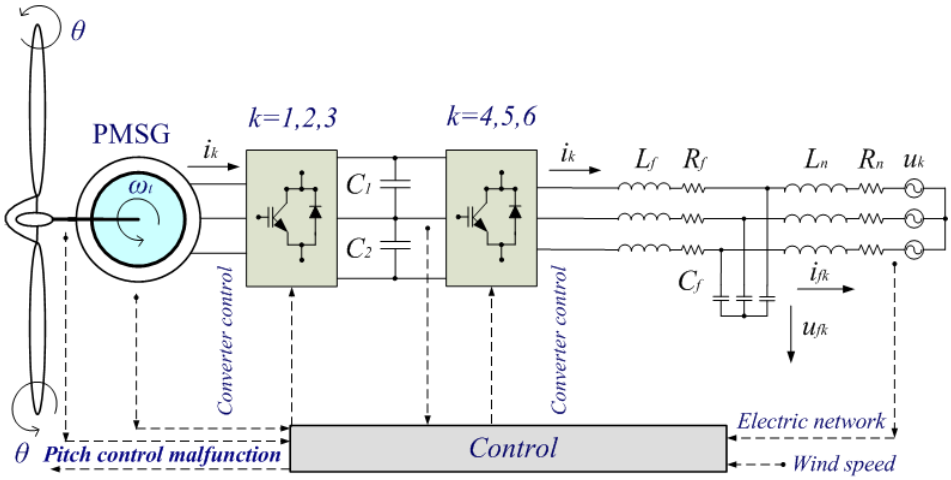

Fig. 2. Wind power system with multilevel converter.

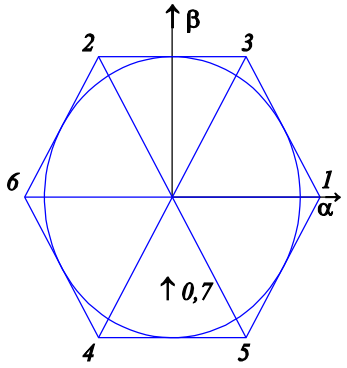

Fig. 3. Output voltage vectors for the two-level converter.

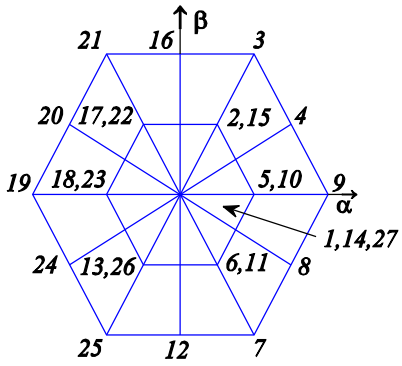

Fig. 4. Output voltage vectors for the multilevel converter.

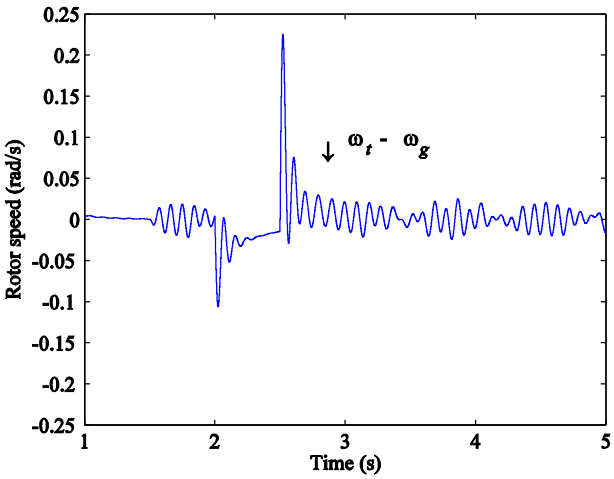

Fig. 5. Relative generator rotor speed to the turbine rotor speed.

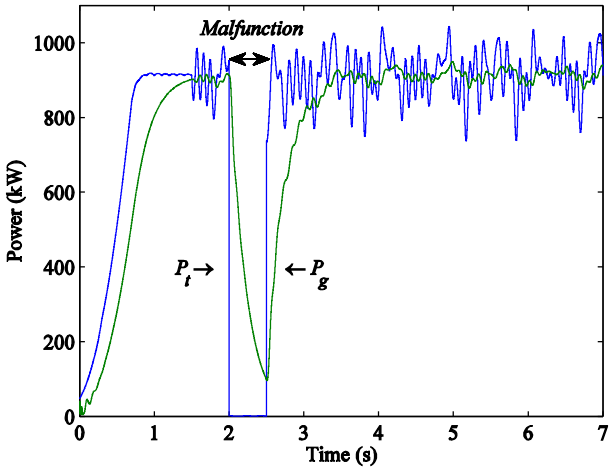

Fig. 6. Mechanical power over the rotor and electric power.

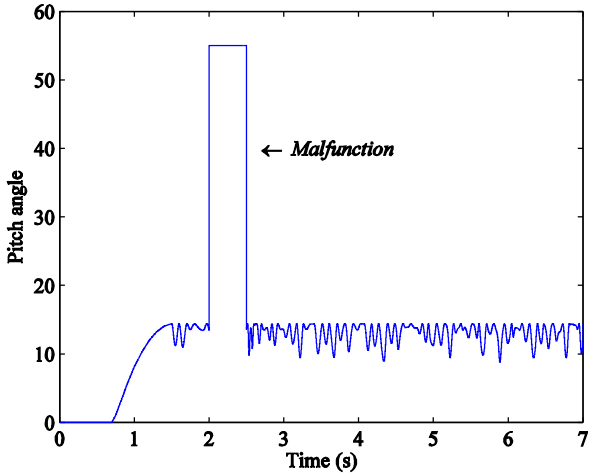

Fig. 7. Pitch angle variation.

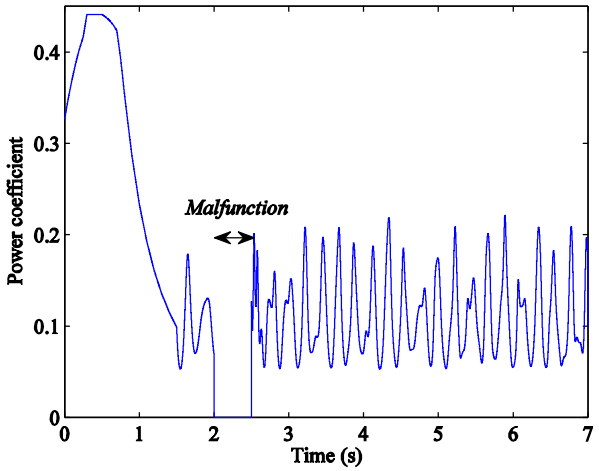

Fig. 8. Power coefficient variation.

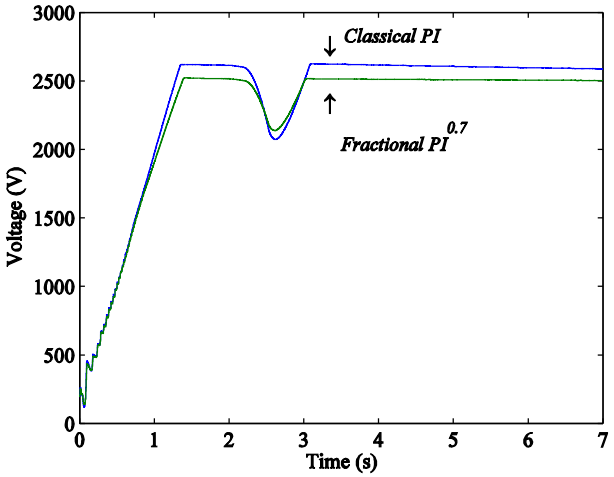

Fig. 9. Voltage v_{dc} for the two-level converter, considering each controller.

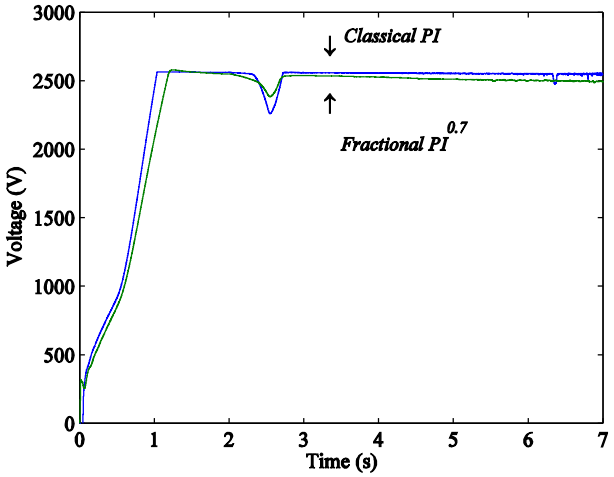

Fig. 10. Voltage v_{dc} for the multilevel converter, considering each controller.

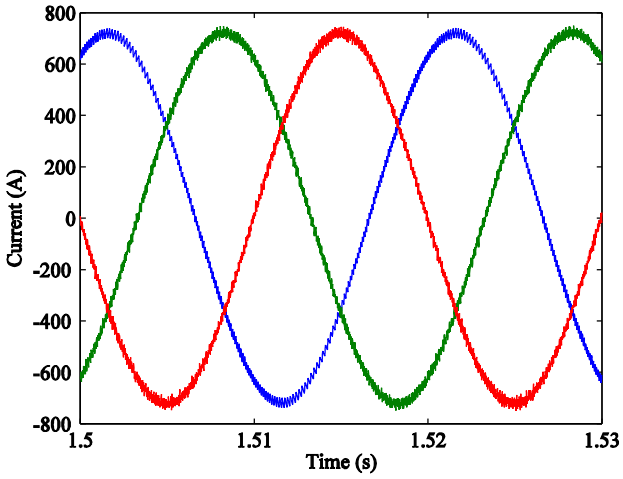

Fig. 11. Output current of the two-level converter.

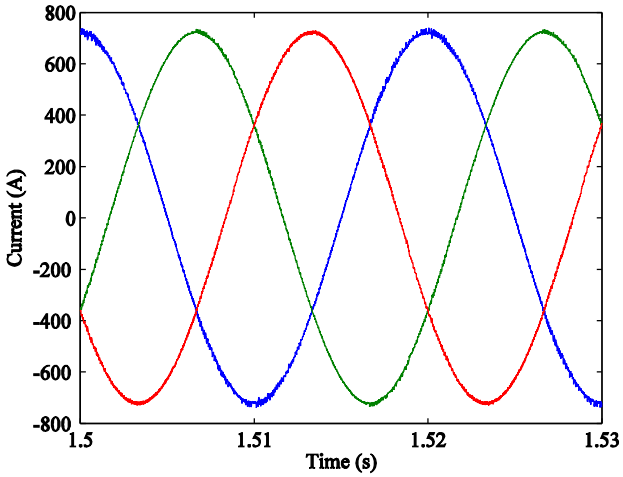

Fig. 12. Output current of the multilevel converter.

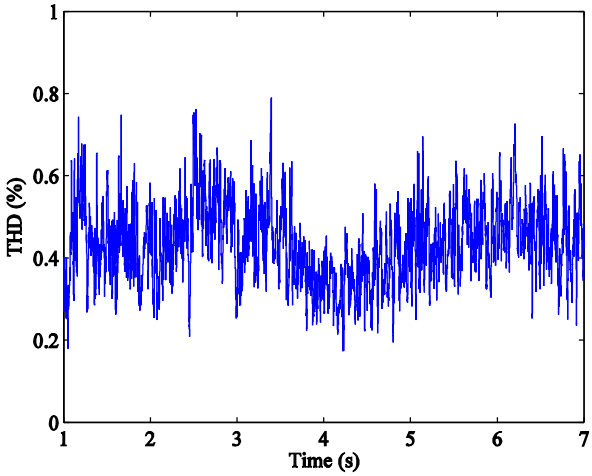

Fig. 13. THD of the current injected in the electric grid with the two-level converter.

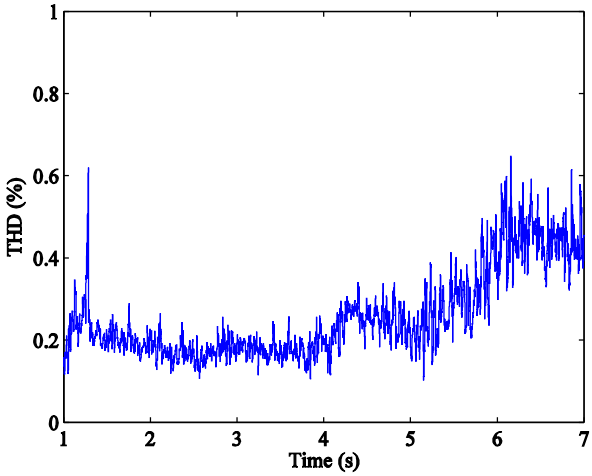

Fig. 14. THD of the current injected in the electric grid with the multilevel converter.

Tables

Table 1

Mechanical eigenswings excited in the wind turbine

k	Source	A_k	ω_k	h_k	m	a_{km}	φ_{km}
1	Asymmetry	0.01	ω_t	1	1	4/5	0
					2	1/5	π/2
2	Vortex tower interaction	0.08	3 ω_t	1	1	1/2	0
					2	1/2	π/2
3	Blades	0.15	9 π	1/2 (g_{11}+g_{21})	1	1	0

Table 2

Output voltage vectors selection for the two-level converter

$\sigma_\beta \setminus \sigma_\alpha$	-1	0	1
-1	4	4;5	5
0	6	0;7	1
1	2	3;2	3

Table 3

Output voltage vectors selection for the multilevel converter, for $v_{C1} > v_{C2}$

$\sigma_\beta \setminus \sigma_\alpha$	-2	-1	0	1	2
-2	25	25	12	7	7
-1	24	13	13;6	6	8
0	19	18	1;14;27	5	9
1	20	17	17;2	2	4
2	21	21	16	3	3

Table 4

Output voltage vectors selection for the multilevel converter, for $v_{C1} < v_{C2}$

$\sigma_\beta \backslash \sigma_\alpha$	-2	-1	0	1	2
-2	25	25	12	7	7
-1	24	26	26;11	11	8
0	19	23	1;14;27	10	9
1	20	22	22;15	15	4
2	21	21	16	3	3

Table 5

Wind power system data

Turbine moment of inertia	2500×10^3 kgm²
Turbine rotor diameter	49 m
Tip speed	17.64-81.04 m/s
Rotor speed	6.9-31.6 rpm
Generator rated power	900 kW
Generator moment of inertia	100×10^3 kgm²

Table 6

Capacitor voltage drop during pitch control malfunction

Controller	v_{dc} (V)	
	Wind power system with two-level converter	Wind power system with multilevel converter
Classical PI	550.6	310.7
Fractional $PI^{0.7}$	380.1	201.3

Table 7

THD of the current injected in the electric grid

Controller	THD (%)	
	Wind power system with two-level converter	Wind power system with multilevel converter
Classical PI	0.91	0.46
Fractional $PI^{0.7}$	0.58	0.13